

Highly Efficient Planar Perovskite Solar Cells through Band Alignment Engineering

Juan Pablo Correa Baena,^{1*} Ludmilla Steier,² Wolfgang Tress,^{2,3} Michael Saliba,³ Stefanie Neutzner,⁴ Taisuke Matsui,⁵ Fabrizio Giordano,² T. Jesper Jacobsson,¹ Ajay Ram Srimath Kandada,⁴ Shaik M. Zakeeruddin,^{1,2} Annamaria Petrozza,⁴ Antonio Abate,² Mohammad Khaja Nazeeruddin,³ Michael Grätzel,² and Anders Hagfeldt^{1*}

¹Laboratory for Photomolecular Science, Institute of Chemical Sciences and Engineering, École Polytechnique Fédérale de Lausanne, CH-1015-Lausanne, Switzerland.

²Laboratory for Photonics and Interfaces, Institute of Chemical Sciences and Engineering, École Polytechnique Fédérale de Lausanne, CH-1015-Lausanne, Switzerland.

³Group for Molecular Engineering of Functional Materials, Institute of Chemical Sciences and Engineering, École Polytechnique Fédérale de Lausanne, CH-1015-Lausanne, Switzerland

⁴Center for Nano Science and Technology@Polimi, Istituto Italiano di Tecnologia, via Pascoli 70/3 20133 Milano, Italy

⁵Advanced Research Division, Panasonic Corporation,1006, (Oaza Kadoma), Kadoma City, Osaka 571-8501, Japan.

JPCB and LS contributed equally to this work.

*Corresponding authors: AH anders.hagfeldt@epfl.ch; JPCB juan.correa@epfl.ch.

Methods

Fs-transient absorption spectroscopy

A Coherent Micra Ti:Sapphire oscillator in conjunction with a Coherent RegA 9040 amplifier (800 nm central wavelength, 40 fs pulse duration and 250 kHz repetition rate) was used to generate pump and probe light. The 520 nm pump beam was generated in a coherent collinear optical parametric amplifier, the probe resulted from white light generation in a sapphire plate. The delay between the two pulses was controlled by a motorized delay-stage and the signal was detected using a photodiode with monochromator, connected to a Stanford Instruments Lock-in Amplifier SR830. During the measurements, the pump beam of 1.6 nJ excitation power was focused on approximately 1 mm² device area. To monitor the current in short-circuit condition, the devices were connected to an Agilent B2912A source/measure unit. All measurements were set up in reflection geometry, measuring double transmission by reflecting the probe beam from the back electrode of the device. To prevent degradation during laser illumination, all measurements were carried out in vacuum, using a continuous flow static exchange gas cryostat (Oxford Instruments Optistat CF).

Band gap estimation measurements

The band gap of the perovskite materials (Supplementary Figure S3) was determined from diffuse reflectance measurements in a wavelength range of 300–900 nm carried out with a UV-3600 spectrometer (Shimadzu Scientific Instruments, USA) that was equipped with an integrating sphere. For these measurements, a thick layer of perovskite was deposited on a quartz slide (Ted Pella, USA) to ensure a good scattering signal. An

absorption coefficient equivalent was calculated after Kubelka-Munk according to

$F(R) = \frac{(1-R)^2}{2R}$ where R is the diffuse reflectance. The band gap was determined from

Tauc plots according to $ah\nu = A(h\nu - E_g)^{\frac{n}{2}}$ with $n = 1$ for a direct band gap material.

The band gaps of SnO₂ and TiO₂ were confirmed by spectroscopic ellipsometry measurements (GES 5E, Sopra S.A., France) in the wavelength range of 250–890 nm on 100 nm thick layers deposited on Si by ALD as described above. The obtained spectra were fitted using a Tauc-Lorentz dispersion law (WinElli II software) to extract the band gap and thickness of the deposited layers. The results were in very good agreement with transmittance measurements performed on films deposited on quartz as well as with literature values.

Photoelectron spectroscopy

The XPS and UPS measurements were performed on a PHI5000 VersaProbe instrument.

The UPS radiation was generated by a He-gas discharge lamp (He I α at 21.22 eV).

The electron binding energy scale was calibrated using the Fermi edge of clean silver.

Samples were prepared in the same way as for the devices for the 2 perovskites on ESLs of SnO₂ and TiO₂, which were deposited on FTO glass.

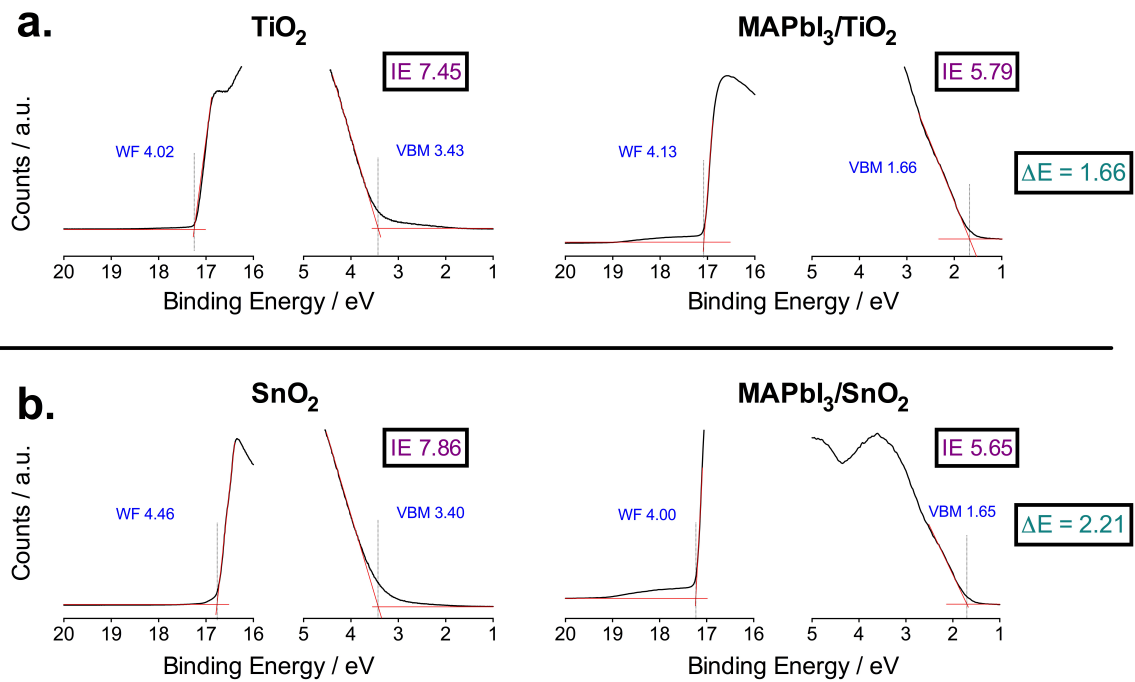


Figure S1. UPS spectra (He I) of the ALD TiO₂ and MAPbI₃ perovskite (a) and ALD SnO₂ and MAPbI₃ (b). Ionization energies (IE) and the difference between the valence band energies (ΔE) of the electron selective layers and the perovskite (ΔE) are shown for all materials.

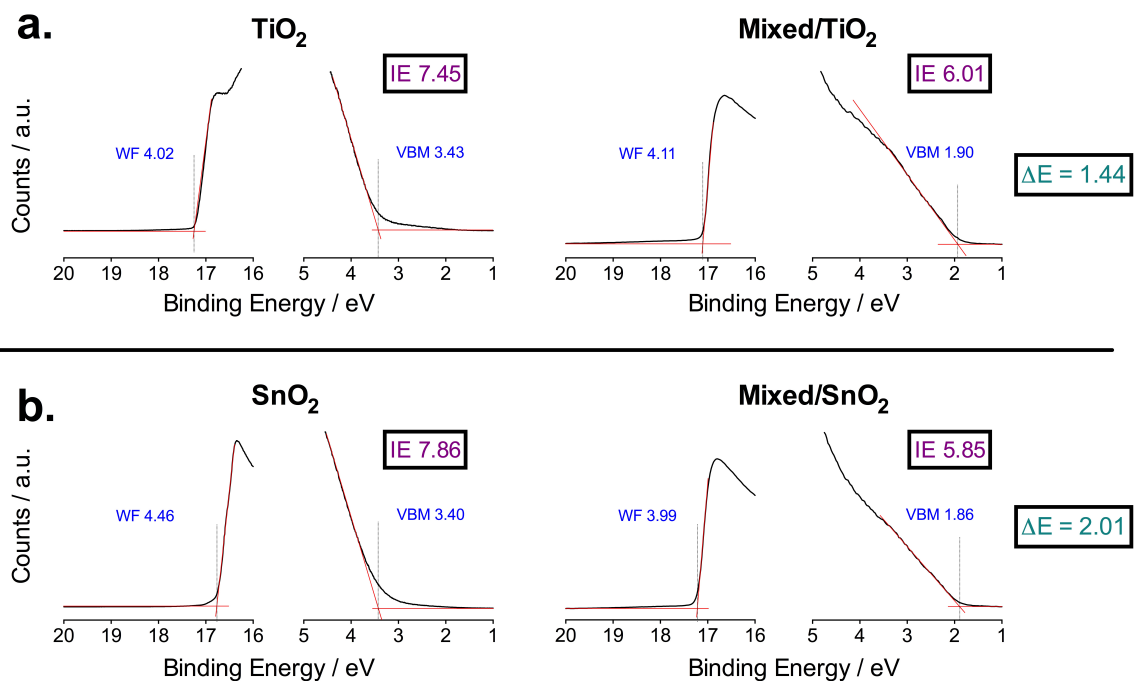


Figure S2. UPS spectra (He I) of the ALD TiO₂ and the (FAPbI₃)_{0.85}(MAPbBr₃)_{0.15} perovskite labeled as ‘mixed’ (a) and ALD SnO₂ and (FAPbI₃)_{0.85}(MAPbBr₃)_{0.15} (b). Ionization energies (IE) and the difference between the valence band energies (ΔE) of the electron selective layers and the perovskite (ΔE) are shown for all materials.

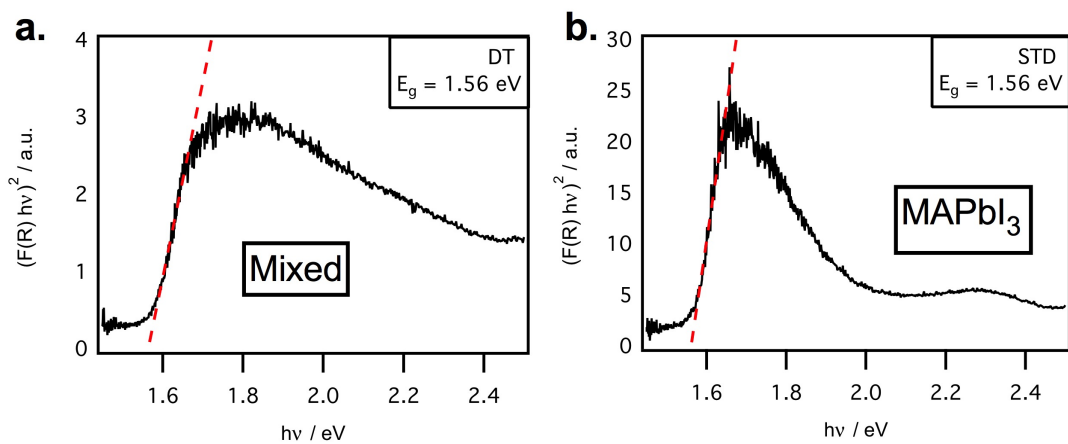


Figure S3. Diffuse reflectance measurements in a wavelength range of 300–900 nm for both the mixed (a) and MAPbI_3 (b) perovskites and their respective optical bandgap.

The band gaps of SnO_2 and TiO_2 were confirmed by spectroscopic ellipsometry measurements in the wavelength range of 250–890 nm on 100 nm thick layers deposited on Si by ALD. The obtained spectra were fitted using a Tauc-Lorentz dispersion law to extract the band gap and thickness of the deposited layers.

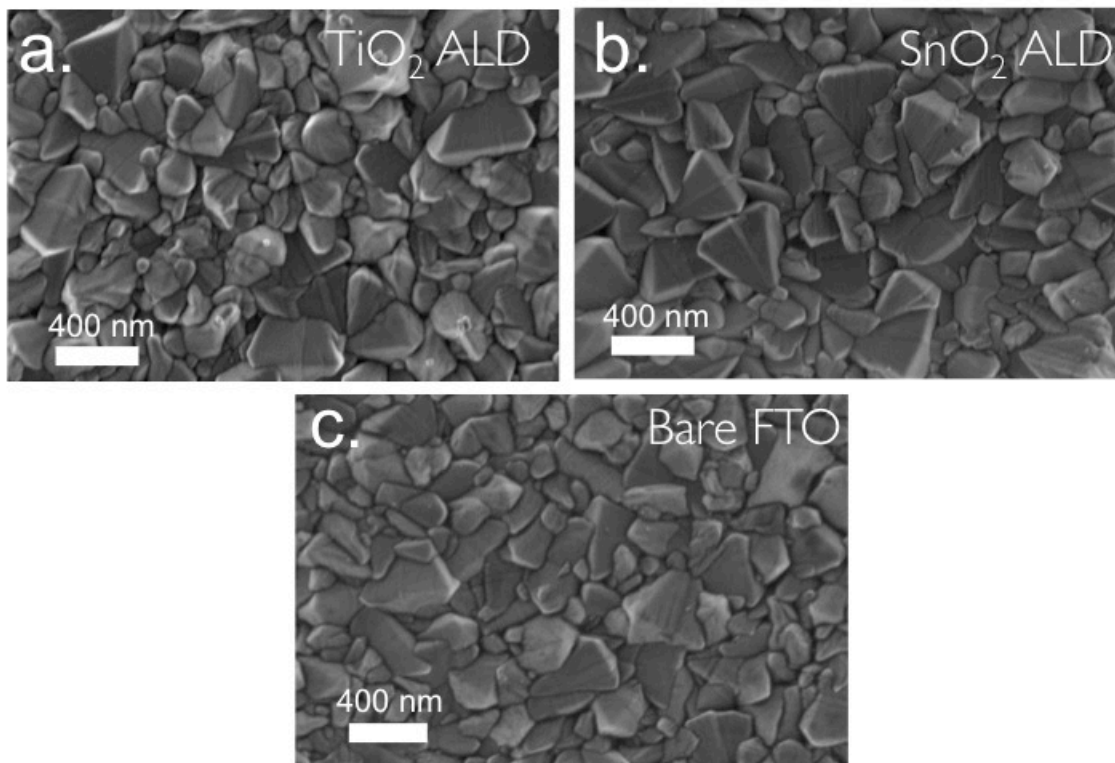


Figure S4. Scanning electron micrographs of FTO substrates coated by atomic layer deposition with a, TiO₂ and b, SnO₂ and compared to c, the uncoated FTO.

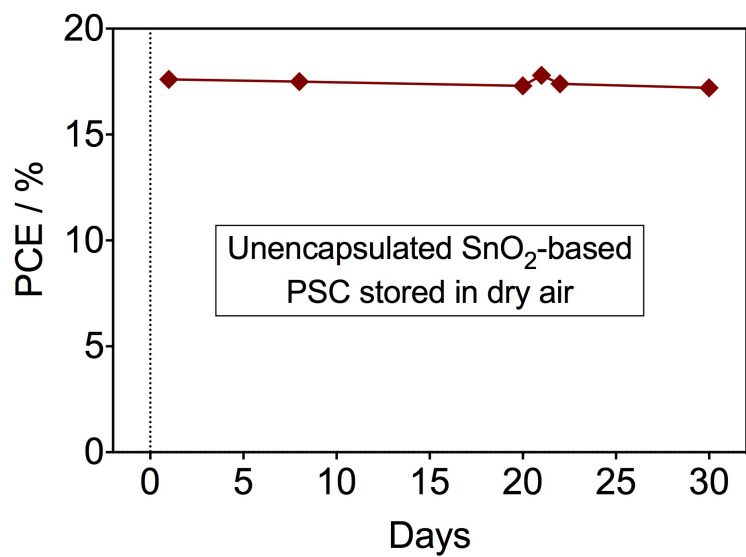


Figure S5. Power conversion efficiency as a function of time for an unencapsulated planar solar cell with a mixed-halide perovskite and a compact layer of SnO₂.

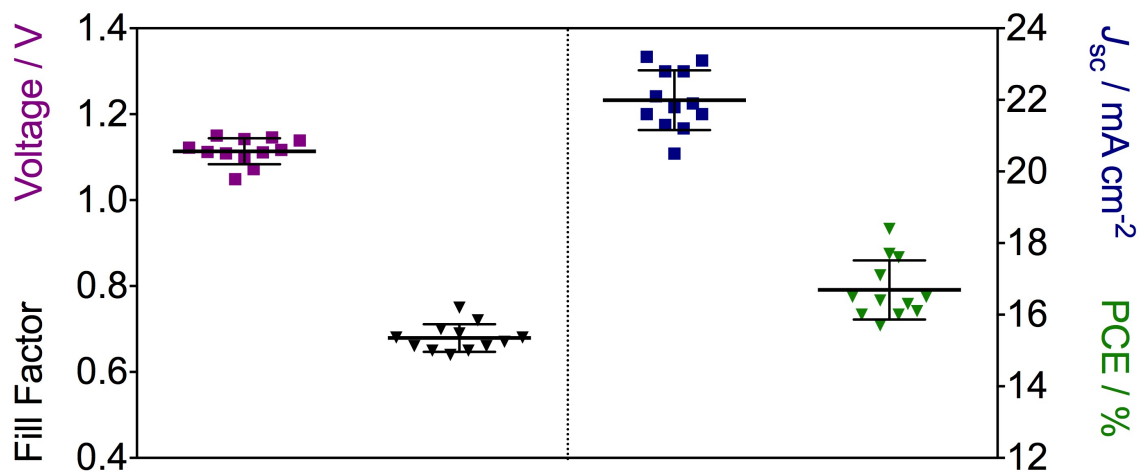


Figure S6. SnO₂ PSC device performance statistics. Open circuit voltage, fill factor, short-circuit current density and power conversion efficiency for 12 different devices.

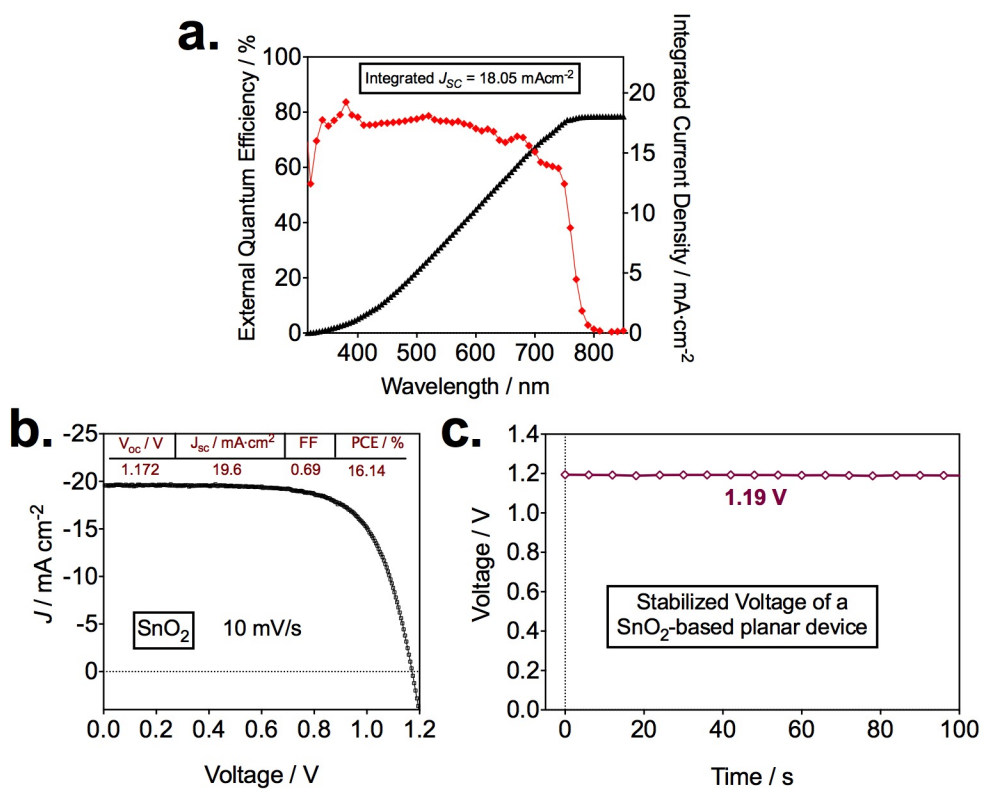


Figure S7. a, External quantum efficiency and integrated current density, **b,** the current-density characteristics of the PSC with the use of a 0.16 cm² mask, **c,** V_{oc} measured over time without the use of a mask, of a SnO₂-based mixed perovskite solar cell.

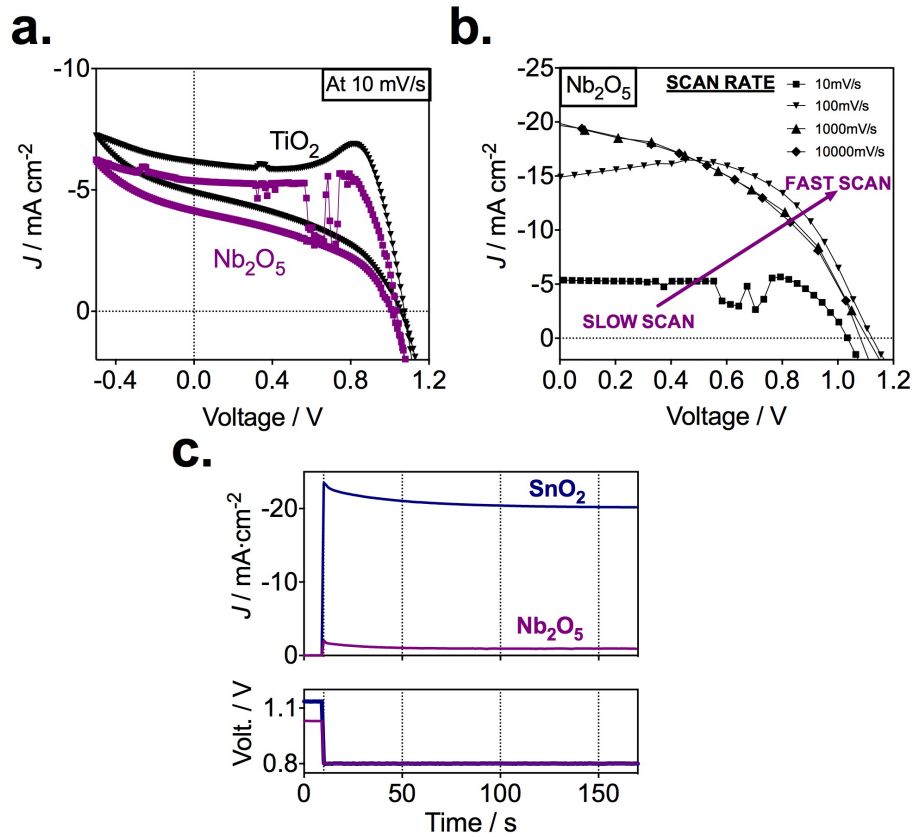


Figure S8. Current-voltage characteristics of a of planar mixed-halide/cation perovskite solar cell based on Nb₂O₅ as the electron selective layer. **a**, Hysteresis behaviour of Nb₂O₅ compared to TiO₂-based planar devices. **b**, Scan rate dependence on current-voltage characteristics for Nb₂O₅ based devices. **c**, Current decays from V_{OC} to maximum power point voltage for SnO₂ and Nb₂O₅ planar systems.

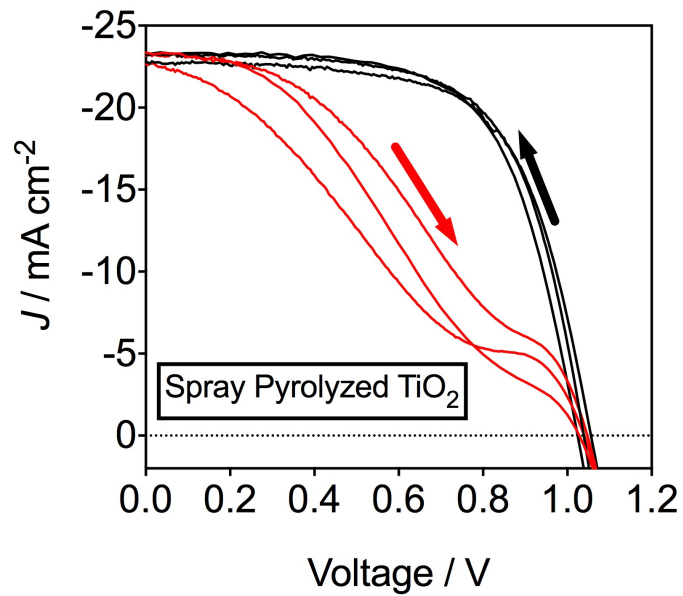


Figure S9. Current-voltage characteristics of a PSC using a spray-pyrolyzed TiO_2 layer (70 nm) as electron selective layer.

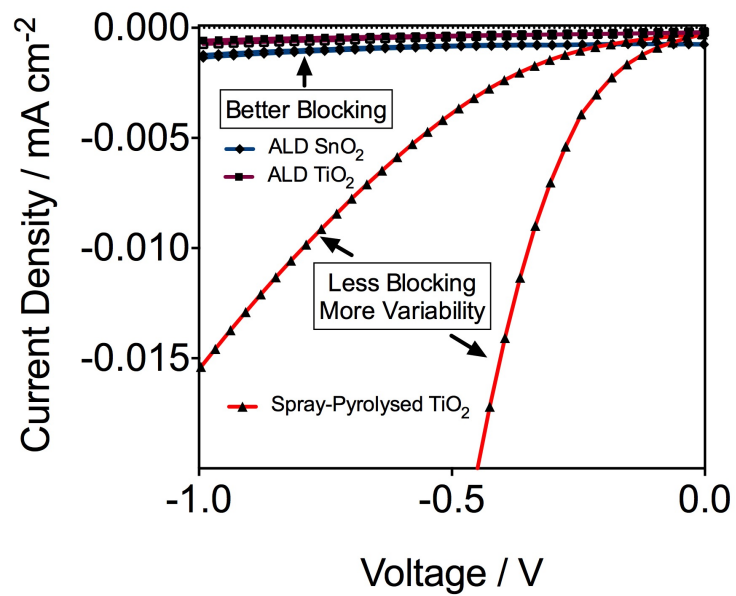


Figure S10. Current-voltage characteristics in dark of devices with the stack configuration of FTO/electron selective layer/Spiro/Gold measured in reverse bias for the three of the ESLs used in this study.

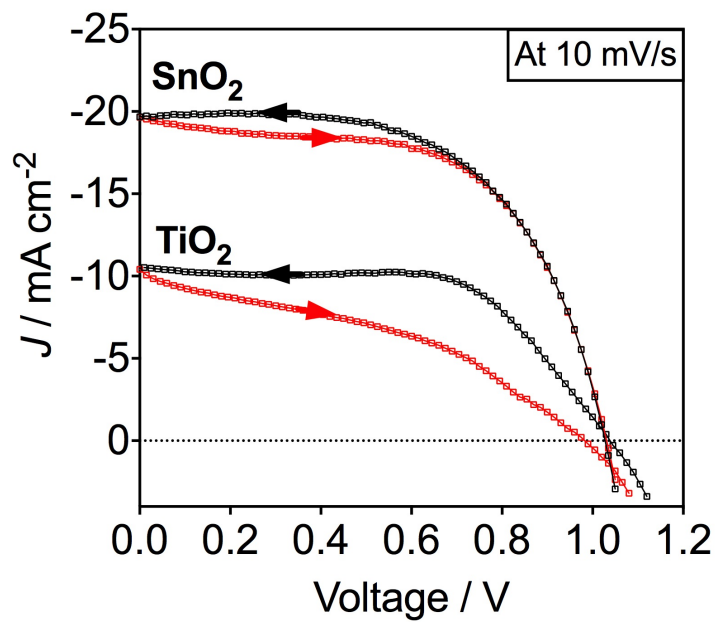


Figure S11. Current-voltage characteristics of a of planar MAPbI_3 perovskite solar cell based on SnO_2 and TiO_2 as the electron selective layers.